

High hydrogen coverage on graphene via low temperature plasma with applied magnetic field



Fang Zhao ^{a,*,1}, Yevgeny Raitsev ^{b,1}, Xiaofang Yang ^c, Andi Tan ^a, Christopher G. Tully ^a

^a Department of Physics, Princeton University, NJ, 08544, USA

^b Princeton Plasma Physics Laboratory, Princeton, NJ, 08540, USA

^c Department of Chemical and Biological Engineering, Princeton University, NJ, 08544, USA

ARTICLE INFO

Article history:

Received 11 October 2020

Received in revised form

4 February 2021

Accepted 22 February 2021

Available online 25 February 2021

Keywords:

Graphene

Cross-field discharge

Hydrogen coverage

Low-temperature

Magnetic field

X-ray photoelectron spectroscopy

ABSTRACT

The chemical functionalization of two-dimensional materials is an effective method for tailoring their chemical and electronic properties with encouraging applications in energy, catalysis, and electronics. One exemplary 2D material with remarkable properties, graphene, can be exploited for hydrogen storage and large on/off ratio devices by hydrogen termination. In this work, we describe a promising plasma-based method to provide high hydrogen coverage on graphene. A low pressure (~10 mtorr) discharge generates a fine-tunable low-temperature hydrogen-rich plasma in the applied radial electric and axial magnetic fields. Post-run characterization of these samples using Raman spectroscopy and X-ray photoelectron spectroscopy demonstrates a higher hydrogen coverage, 35.8%, than the previously reported results using plasmas. Plasma measurements indicate that with the applied magnetic field, the density of hydrogen atoms can be more than 10 times larger than the density without the magnetic field. With the applied electric field directed away from the graphene substrate, the flux of plasma ions towards this substrate and the ion energy are insufficient to cause measurable damage to the treated 2D material. The low damage allows a relatively long treatment time of the graphene samples that contributes to the high coverage obtained in these experiments.

© 2021 Elsevier Ltd. All rights reserved.

1. Introduction

Graphene, a two-dimensional honeycomb lattice with a sp^2 carbon bond structure, offers a radically new platform for electronic and photonic science and technology based on its exceptional electronic, mechanical, and optical properties [1–3]. Graphene is a zero-gap semiconductor with a linear energy-momentum dispersion relation and the charge carriers behave like massless Dirac fermions [4]. However, the absence of a sizeable bandgap around the Fermi level has severely limited the application of graphene in microelectronic devices. To date, the desire to opening a bandgap [4,5] in graphene has given rise to intense studies in both theoretical [6,7] and experimental works [8]. Two major routes to introduce bandgap in graphene are forming graphene nanostructures [7] and chemical modification [8]. It is extremely

challenging to fabricate graphene nanostructures, including nanoribbons [9] and nanopores [10], with reliable control at the nanometer scale. In contrast, the chemical modification of the graphene surface is more practical for industrial applications because it is compatible with large scale processing. In particular, one promising chemical approach to modify the chemical and electronic properties of graphene is the exposure to hydrogen plasma [11,12] or hydrogen annealing [13] to induce hydrogen chemisorption on the carbon lattice with sp^3 hybridization. Moreover, observations on hydrogenated graphene have shown that hydrogen can be removed with the annealing process at modest temperatures [12], suggesting a weak chemical covalent bond between graphene and hydrogen. This advocates graphene as an alternative material for hydrogen storage.

Hydrogenation by plasma is a promising technique to induce hydrogen chemisorption on graphene due to the high reactivity of hydrogen radicals and compatibility with standard wafer-scale microfabrication techniques. However, in conventional direct-current (DC) and radio-frequency (RF) plasma processing reactors, high energy hydrogen ions and energetic atoms generated due to charge-exchange collisions between ions and atoms can

* Corresponding author. Department of Physics, Jadwin Hall, Princeton, NJ, 08544, USA.

E-mail address: fangz@princeton.edu (F. Zhao).

¹ These authors contributed equally.

induce substantial damage on graphene surface by irreversible etching and sputtering [14]. This drawback limits the applicability of the plasma-based graphene hydrogenation. Elias et al. showed the first study on hydrogenation of suspended graphene using DC plasma by hydrogen/argon gas mixture for several hours and achieved 10% hydrogen coverage [15]. Larger hydrogen coverages of graphene (e.g. 16.67% [12] and 33% [16]) were achieved with RF hydrogen plasma. However, graphene with low damage was only possible to achieve with a relatively short exposure (~1 min) of graphene samples to this plasma. There is also a report on 33% hydrogen coverage using electron-beam-generated plasma confined by the applied magnetic field, while no dehydrogenation process was applied to confirm the damage situation [17]. In this work, it is shown that the use of a hydrogen plasma generated by energetic electrons in crossed electric and magnetic fields (so-called cross-field or ExB plasma discharge [18–20]) can provide a higher hydrogen coverage than the above studies. The cross-field discharge yields a high density of hydrogen atoms which can be modified with an adjustable magnetic field. We explored the treatment of graphene samples by changing variables such as magnetic field, sample location, and plasma duration. Plasma properties were characterized by electrostatic Langmuir probes [19,21] and optical emission spectroscopy (OES) [22]. Hydrogenated graphene samples were characterized by Raman spectroscopy and X-ray photoelectron spectroscopy (XPS). High hydrogen coverage of 35.8% on monolayer graphene was achieved by 30 min 11 Gauss (G) plasma. Furthermore, bi-layer and tri-layer graphene were studied as well and subsequent thermal annealing processes show evidence for reversible hydrogenation. Hydrogen is more likely to bond on multi-layer graphene, reaching 45% on tri-layer graphene, due to lower surface barrier energy. Herein, we demonstrate that the use of ExB plasma discharge enables to achieve a high value of hydrogen coverage with low damage to the graphene.

2. Material and methods

2.1. Preparation of graphene sample on SiO₂/Si

Graphene (provided from Graphenea Inc.) was synthesized by chemical vapor deposition (CVD) on Cu foils, including monolayer, bi-layer, and tri-layer graphene. The MMA resist was used as the carrier layer during the wet chemical transfer process. The MMA/graphene/copper foil was floated on the surface of a solution of 0.5 M ammonium persulfate (Aldrich, >98%) at room temperature for 2 h to etch the copper foil. After the copper was etched, the block was rinsed in DI water and transferred onto a SiO₂/Si substrate. The transferred substrate was dried in the air for 15 min. Finally, the MMA carrier layer was dissolved in acetone firstly at 70 °C for 2 h, then at room temperature overnight. Before to be loaded in the plasma chamber, the graphene/SiO₂/Si samples were annealed in Ar/H₂ (5% of H₂) at 150 °C for 6 h to burn off the MMA residue.

2.2. Plasma hydrogenation

Hydrogen plasma was generated by the energetic electrons extracted from RF-plasma cathode to the reactor chamber in which radial electric and axial magnetic fields are applied as shown in Fig. 1. This cross-field plasma discharge is described in detail elsewhere [18–21]. The RF cathode is electrically insulated from the reactor chamber that allows the DC voltage biasing of the chamber with respect to the cathode to generate the plasma in the chamber [20]. A set of electromagnet coils are placed in a Helmholtz configuration (Fig. 1) to produce a nearly uniform magnetic field along with the reactor chamber. In the operation of the cross-field discharge, the

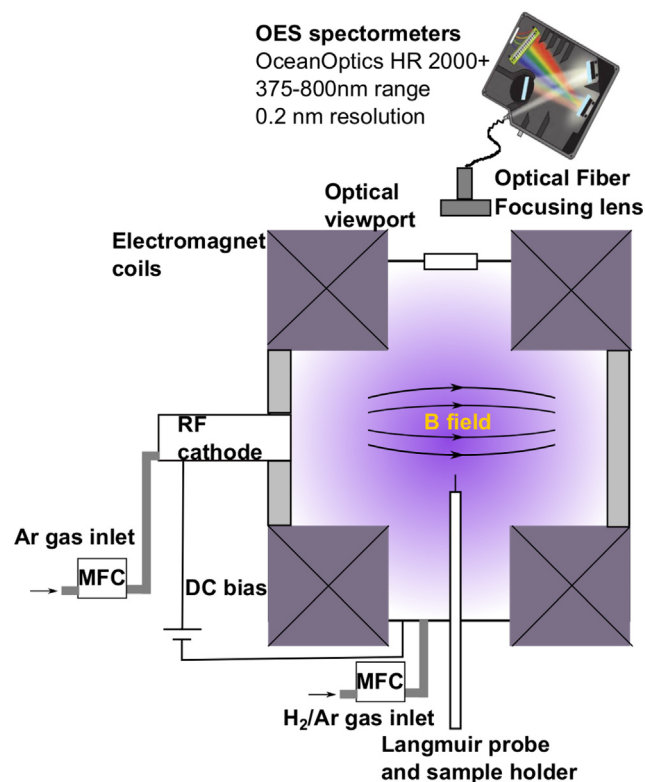


Fig. 1. Low-temperature crossed-field plasma discharge system setup. (A colour version of this figure can be viewed online.)

applied DC bias extracts electrons from the plasma cathode to the reactor chamber where a low-temperature magnetized plasma is formed by impact ionization of energetic electrons with neutral gas atoms and molecules. The applied magnetic field keeps the electron flow along the field lines. Nevertheless, electrons can diffuse across the magnetic field towards the reactor chamber wall (acting as the anode) due to scattering induced from collisions with heavy plasma species (ions, atoms, and molecules) and plasma fluctuations [18,19]. The applied electric field between the reactor chamber and the RF cathode keeps ions away from reaching the chamber wall. The operation details are in Supplementary material 1.

2.3. X-ray photoelectron spectroscopy (XPS)

The XPS analysis of graphene samples was conducted using a ThermoFisher K-Alpha X-ray Photoelectron Spectrometer. The system is equipped with a monochromated Al K α X-ray radiation source (1486.6 eV) and a focusing lens allowing for analysis area from 30 to 400 μ m in 5 μ m steps. In this study, we selected a 400 μ m X-ray spot for all XPS measurements. Survey spectra were taken at 200 eV pass energy and the high-resolution spectra for the C 1s region was recorded at 20 eV pass energy. The XPS system has been calibrated using the Au 4f_{7/2} (84.0 eV) signal from freshly Ar⁺ sputtered samples. The XPS data was analyzed with CasaXPS (Casa Software Ltd.). A Shirley-type background was subtracted from the raw photoemission data. The individual peaks were fitted by a Gaussian-Lorentzian (GL(30)) function with the FWHM between 0.8 and 1.2 eV.

2.4. Raman spectroscopy

The graphene sheets on SiO₂ were characterized by Raman

spectroscopy on a Horiba Jobin-Yvon LabRAM Aramis Raman system using a 100× objective lens with a numerical aperture (NA) of 0.95. The excitation source for Raman spectroscopy is a 532 nm laser (2.33 eV) with a laser power of 0.6 mW to avoid laser-induced heating. The acquisition time is 10 s with 5 accumulations.

2.5. Atomic force microscopy (AFM)

AFM measurements were carried out in tapping mode on AFM nanoman system. The tips are 1–10 Ohm/cm n doped Si with a resonant frequency of 331–340 kHz and a spring constant of 20–80 N/m from Veeco (RTESP). The surface roughness was determined by AFM mapping using a $5 \times 5 \mu\text{m}^2$ area with a 512×512 pixel resolution.

2.6. Annealing of hydrogenated graphene

Annealing of samples of hydrogenated graphene was carried out in a quartz tube furnace. The samples were loaded in a ceramic boat. After the pressure reached 1 mTorr, Ar gas flow with 100 sccm was introduced into the tube to 1 atm. The annealing process was 3 h long at 500 °C.

2.7. Plasma analysis

To understand the mechanism of the hydrogenation, spatial variations of the electron energy probability function (EPPF) were measured using an electrostatic Langmuir probe with and without the magnetic field. The probe system used in this experiment is described in Ref. [20]. In addition to spatial variations of plasma properties, the chemical composition of the plasma was determined using optical emission spectroscopy (OES). For that purpose, an OceanOptics 2000-HR spectrophotometer was used to collect the spectra through a viewport flange on the reactor chamber (Fig. 1) [22]. More details can be found in the Supplementary material.

3. Results and discussion

3.1. Characterizations of monolayer and multi-layer graphene before and after plasma treatment

Before discussing the hydrogenated graphene, we wish to stress two main points that must be considered for the sake of clarity. Firstly, no pure graphane or graphone has been synthesized yet and all the reported experimental products are partially hydrogenated graphene. Secondly, it is difficult to measure the percentage of hydrogen on graphene films by most surface techniques. Indeed, surface characterization techniques, such as Raman spectroscopy, Fourier-Transform infrared spectroscopy (FTIR), and XPS, provide indirect information based on assumptions, educated guesses, and assignments. However, FTIR is not suitable for ambient exposing monolayer graphene samples owing to the weak thin film signals and amorphous carbon coating on the surface. In this study, we analyzed all the samples by Raman spectroscopy and XPS with unified assignments to seek reliability. Pristine monolayer graphene on SiO₂ was characterized by Raman spectroscopy and XPS as shown in Fig. S1 to confirm the graphene quality. To estimate the effective plasma condition, graphene samples were treated at different plasma chamber locations, magnetic field values, and process durations (Figs. S1d, e, f). The plasma treatment of 30 min 11 G plasma was chosen in the study. To understand the effect of the magnetic field, 30 min 0 G plasma treatment was appointed as the control measurement. The samples were located at 10 cm, 14 cm, and 18 cm away from the chamber axis to the sample holders.

3.1.1. Raman spectroscopy analysis

Raman spectroscopy has served as a powerful tool in characterizing graphene thickness, defects, and lattice strain. However, its quantitative use is limited for graphene grown on Cu because of strong metallic photoluminescence that interferes with Raman signals. Fig. S1a shows one Raman spectra of hydrogenated graphene on Cu with strong photoluminescence. The electronic interactions between graphene and the metallic substrates may modify the effective Fermi velocity of graphene, and thus affect the double resonance excitation of 2D peak [23]. To avoid such photoluminescence for Raman peak quantitative analysis, the graphene was transferred to the SiO₂/Si substrates in our study. Hydrogenation results in the appearance of D and D' bands, slight broadening and a decrease of the intensity of the 2D band relative to the G band in Raman spectra. The D band at 1340 cm⁻¹ and the D' band at 1620 cm⁻¹ are assigned as graphene defects activated via an intervalley double-resonance Raman process [24]. The observation of D and D' indicates that the defects are introduced in the graphene lattice by the plasma treatment. All of the graphene samples treated by 30 min 11 G and 30 min 0 G plasma at 10 cm, 14 cm, and 18 cm locations were recovered back to pristine graphene state after dehydrogenation annealing. The defects are mainly caused by the hydrogenation of graphene, which results in breaking the symmetry of C=C sp² bonds to form C-H sp³-like bonds. The D band allows indirect estimation of the extent of hydrogenation by considering each C-H bond as an sp³-like impurity on the lattice, but with little justification. The integrated intensity of the D band (I_D) can be used to estimate the size of defect-free areas (L_a) in the film when related to the integrated intensity of the G band (I_G) and the wavelength in nm of the Raman excitation energy (λ) (Eq. (1)) [25].

$$L_a = 2.4 \times 10^{-10} \lambda^4 \left(\frac{I_D}{I_G} \right)^{-1} \quad (1)$$

As shown in Fig. 2a and c, the I_D/I_G ratios of graphene samples in the 30 min 11 G plasma treatment increase following the sample holders getting closer to the chamber axis. However, without the magnetic field, the I_D/I_G ratio is independent to different locations and overlaps, as shown in Fig. 2b and c. Referring to Eq. (1), the domain sizes L_a of hydrogenated graphene films are estimated in Table 1.

3.1.2. X-ray photoelectron spectroscopy and atomic force microscopy analysis of monolayer graphene

To precisely determine the hydrogen coverage, the XPS data is analyzed with a Shirley background subtraction and fitted by Gaussian-Lorentzian line shape. In the C 1s core-level scan, the hydrogenation coverage η, the atomic hydrogen to carbon ratio in percent, corresponds to

$$\eta(\%) = 100 \frac{C3}{C1 + C2 + C3} \quad (2)$$

The parameters of C1, C2, and C3 denote the areas under the relevant constituents of C 1s spectrum shown in Fig. 2d and e [26,27]. We assign C1 as unhydrogenated carbon atoms sp² at 284.4 eV (green peak), C2 as the three nearest neighboring unhydrogenated C atoms adjacent to one C-H bond at 284.0 eV (yellow peak), and C3 as the C atoms with hydrogen attached in an sp³-like configuration at 285.1 eV (blue peak) [26]. The rest of the other components are carbon-oxygen components, including hydroxyl (C-OH, 285.7 eV), epoxy (C-O-C, 286.7 eV), carbonyl (C=O, 288.0 eV), and carboxyl (O-C=O, 289.1 eV) [28]. Hydrogen plasma has been reported to remove sticky residues composed of MMA and

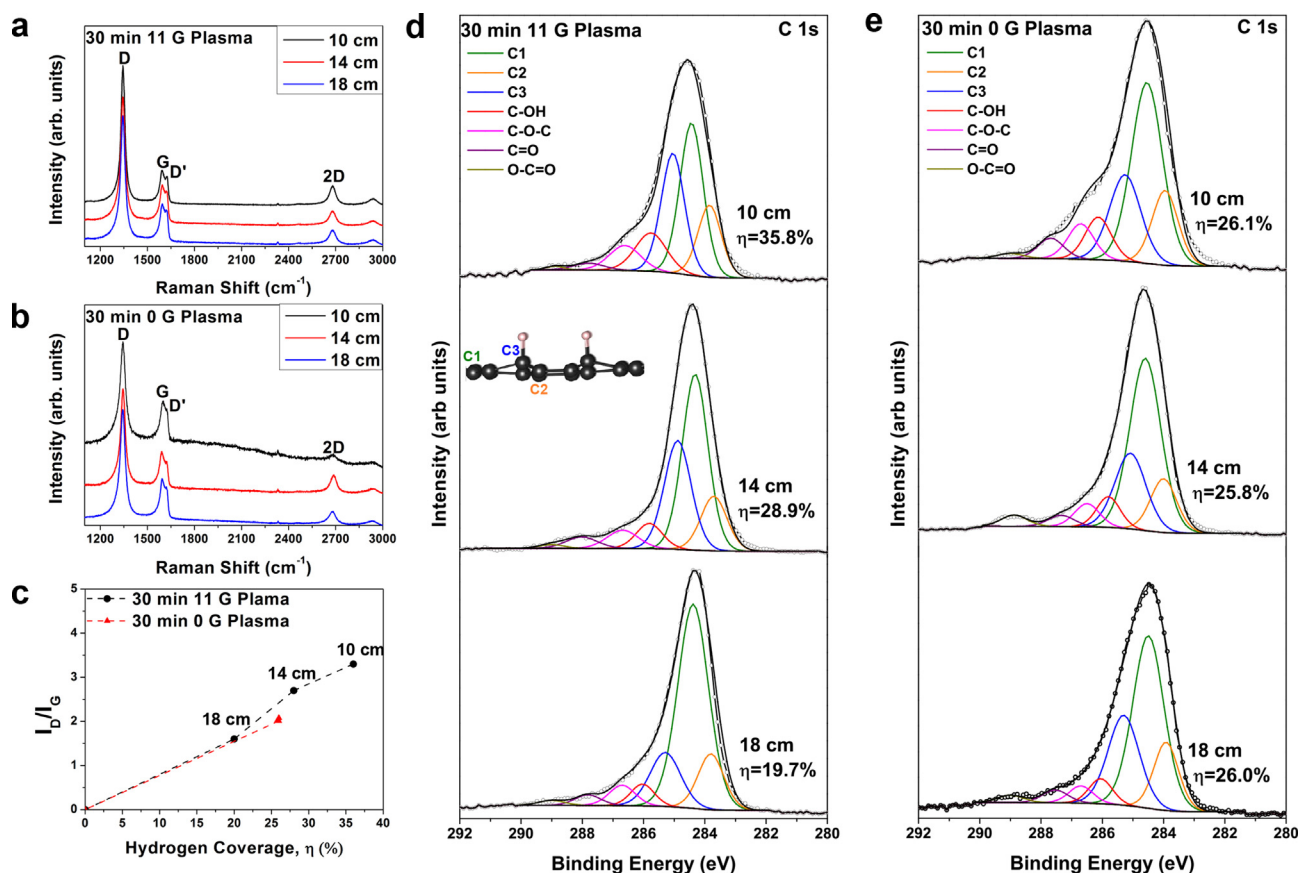


Fig. 2. Raman spectra of monolayer graphene after 30 min 11 G plasma (a) and 30 min 0 G plasma (b) treatments at different sample locations away from the chamber axis to sample holders. (c) the ratio of integrated intensity, I_D/I_G , in the Raman spectra as the function of the hydrogen coverage determined by XPS. The XPS C 1s core-level spectra of graphene after 30 min 11 G plasma (d) and 30 min 0 G plasma (e) treatments. The green peak (graphene sp^2 peak) is C1 at 284.4 eV, the yellow peak (the nearest neighbor C atoms to a C–H bond) is C2 at 284 eV, the blue peak (C–H bonds sp^3 -like peak) is C3 at 285.1 eV, and the rest peaks are the carbon-oxygen components [26]. A schematic inset of C1, C2, C3's positions is shown in (d). (A colour version of this figure can be viewed online.)

Table 1

The size of defect free areas L_a and hydrogen coverage of graphene samples treated by plasma.

Plasma condition	30 min 11 G Plasma			30 min 0 G Plasma		
Sample location	10 cm	14 cm	18 cm	10 cm	14 cm	18 cm
I_D/I_G	3.3	2.7	1.6	2.01	2.03	2.02
L_a (nm)	5.80	7.12	12.01	9.56	9.47	9.51
η	35.8%	28.9%	19.7%	26.1%	25.8%	26.0%

Si-based nanoparticles on graphene surface [29]. The XPS survey scans in Fig. S2 show that the ratio of C/O increases after the plasma

treatment owing to the removal of residues by hydrogen plasma, which is consistent with the AFM surface morphology analysis shown in Fig. 3. The surface root mean square (RMS) roughness of the clean SiO_2/Si substrate is 0.21 nm. Fig. 3b reveals that MMA residual contamination (white spots) presents on the graphene surface after the wet transfer and annealing processes with the RMS 0.71 nm. After plasma treatment, the RMS of graphene surface decreased to 0.23 nm and no apparent damage was observed. The carbon-oxygen components of hydrogenated graphene samples are primarily from air exposure. The XPS peak location, the full width at half maximum (FWHMs), and the peak area percentage of monolayer graphene after plasma treatments with and without magnetic

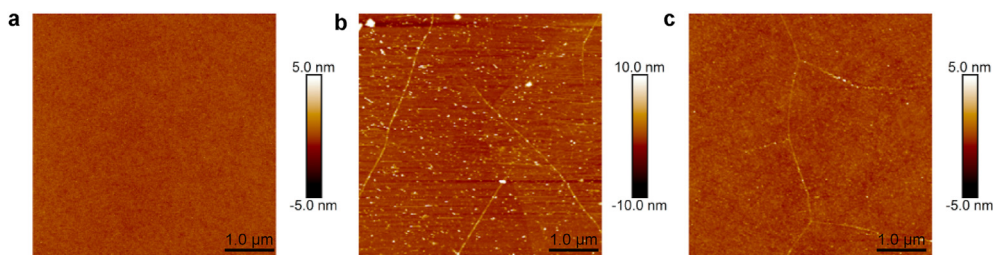


Fig. 3. AFM topography map of the SiO_2/Si substrate (a), CVD graphene transferred on SiO_2/Si before hydrogen plasma treatment (b) and after 30 min 11 G plasma treatments located at the 10 cm away from the chamber axis to sample holders (c). (A colour version of this figure can be viewed online.)

field are shown in Table S1. After 30 min 11 G plasma treatments, the η increases from 19.7% to 35.8% as the sample is placed closer to the plasma center. Nevertheless, the η for samples treated by zero magnetic field plasma is independent of different sample locations, with values around 26.0%. The hydrogen coverages determined by XPS are in good agreement with the I_D/I_G ratio of Raman spectra and the size of defect free area (Fig. 2c and Table 1). In our study, a gas mixture of Ar/H₂ was applied as the hydrogen source for the plasma, as opposed to pure hydrogen gas. With the addition of the Ar gas, it is easier to run the hydrogen content plasma to generate and sustain the plasma, as Ar has a larger ionization cross section than hydrogen molecules and unlike hydrogen molecules, does not involve energy losses on dissociation and molecular excitation. On the other hand, the Ar ions could cause a stronger sputtering of the graphene than hydrogen to create irreversible defects. Considering the effect of the Ar plasma ions, the dehydrogenation thermal annealing process was studied. After annealing in Ar for 3 h at 500 °C, the Raman and XPS spectra of three samples treated by 30 min 11 G Ar/H₂ plasma were recovered back to the pristine graphene state and no new peak appeared which indicates no new materials crystallinity was created during annealing, as shown in Fig. S3. The reversible dehydrogenation behavior verifies the low damage induced by the low-temperature plasma.

3.1.3. X-ray photoelectron spectroscopy analysis of multi-layer graphene

Further characterization studies have been done on bi-layer and tri-layer graphene. Raman spectra of multi-layer samples are shown in Fig. S4. Bi-layer and tri-layer graphene have a broader redshifted 2D band and a slight blue-shifted G band [24]. After hydrogen plasma treatment, the analysis of XPS of samples at the 10 cm location is shown in Fig. 4. Defect-free graphene is widely considered to be completely impermeable to all gases and liquids. Geim's group shows that monolayer graphene is permeable to thermal protons and hydrogen molecules, whereas hydrogen permeation was observed at a high pressure of hydrogen (750 torr) on free-standing monolayer graphene through three days [30,31]. No proton and hydrogen transport was detected for bi-layer graphene [31]. In this study, graphene was supported on SiO₂/Si and the hydrogen plasma was carried out at a low pressure (mtorr range) and 30 min, suggesting that hydrogen is unlikely to permeate through bi-layer and tri-layer graphene. We assume that the XPS C–H sp³-like signal is only from the top layer of graphene. The XPS intensity data is evaluated from different thickness measurements. Considering the different thickness of graphene on a substrate (SiO₂/Si), the intensity of overlayer-originated photoemission peak [32] is:

$$I_t(\theta) = I_t^\infty(\theta) \left[1 - \exp\left(\frac{-t}{\lambda \cos(\theta)}\right) \right] \quad (3)$$

where I_t^∞ is the peak intensity from the clean substrate. Here λ represents the electron attenuation length (EAL), t is the overlayer (graphene) thickness and θ is the angle between the surface normal and electron emission direction. The EAL values are list in Table S2. In our study, at a monochromated Al K α X-ray radiation source (1486.6 eV), C 1s with a kinetic energy of 1200 eV has the λ of 3.05 nm through few-layer graphene on SiO₂/Si [32–34]. The electron escape depth d ($d = \lambda \cos\theta$ and $\theta = 0^\circ$) is 3.05 nm and the thickness of a single layer of graphene is 0.335 nm [34]. We estimate that the signal from the top graphene layer contributes (γ) 52.8% and 37% from the sp² intensity components of the bi-layer and tri-layer graphene, respectively. Therefore, the hydrogen coverage of multi-layer is

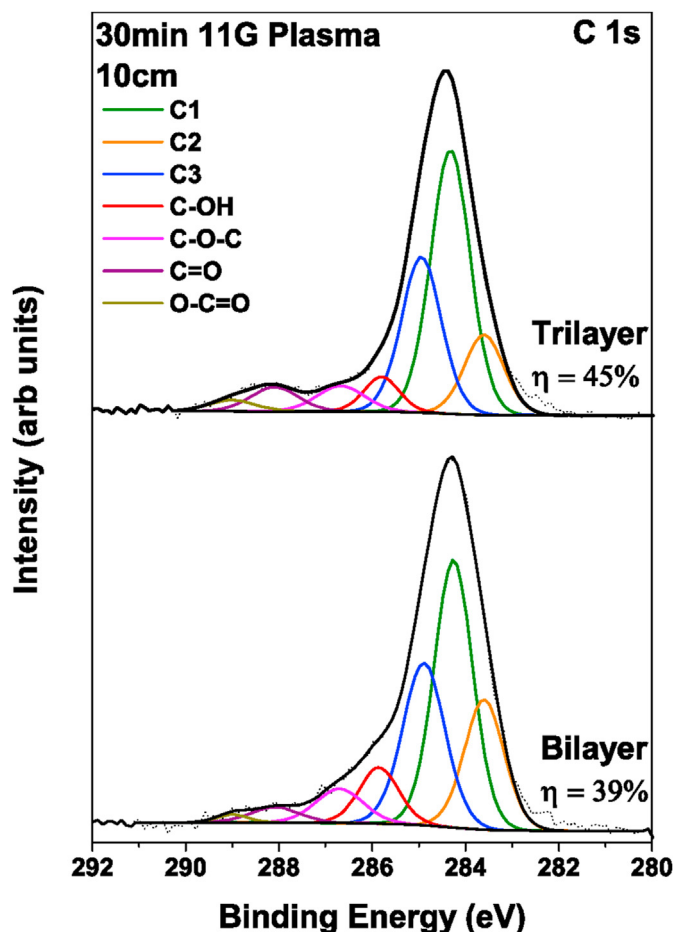


Fig. 4. XPS C 1s core-level of bi-layer and tri-layer graphene located at the 10 cm away from the chamber axis to sample holders after plasma 30 min 11 G plasma treatment. (A colour version of this figure can be viewed online.)

$$\eta(\%) = 100 \frac{C3}{\gamma C1 + C2 + C3} \quad (4)$$

In this study, the XPS scan area was chosen according to optical microscopy images to avoid visible defects. We assume the scan areas of multi-layer samples are defect-free and the hydrogen coverages are 39% for bi-layer graphene and 45% for tri-layer graphene. The XPS results indicate that hydrogenation is more likely to bond on bi-layer and tri-layer graphene than monolayer graphene. Under the same plasma condition, the different hydrogen coverage is caused by the different surface hydrogenation barrier. The hydrogenation barrier of bi-layer and tri-layer is similar to graphite, about 0.2 eV, while that of the monolayer is 0.53 eV [12]. The hydrogenation of the bi-layer and tri-layer graphene is more feasible than that of the monolayer graphene on SiO₂/Si due to the lower hydrogenation barrier on bi-layer and tri-layer graphene.

3.2. Characterization of the hydrogen plasma

Fig. 5 shows the results of probe measurements during the operation of the cross-field discharge with the above specified Ar/H₂ gas mixture. The results are compared for the plasma operation with the applied magnetic field of 11 G and without the magnetic field. Electrostatic probe measurements were conducted at two different locations of the reactor chamber – at R = 0 cm of chamber center, i.e. on the chamber axis and in front of the RF cathode, and

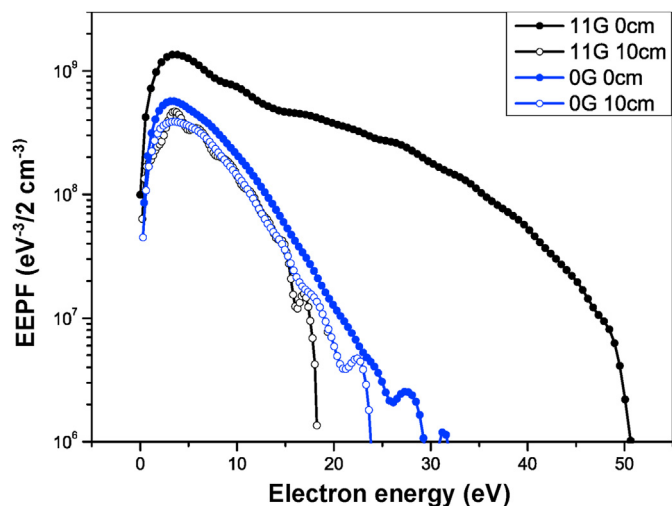


Fig. 5. Plasma electron-energy probability function (EEPF) in the Ar/H₂ gas mixture plasma with (11 G, black) and without (0 G, blue) magnetic field at two different locations: 0 cm of the chamber on the chamber axis and in front of the RF cathode, and 10 cm away from plasma axis where the graphene samples (with highest hydrogen coverage). (A colour version of this figure can be viewed online).

at $R = 10$ cm where the graphene samples with the highest hydrogen coverage were exposed to the plasma. The most dramatic difference between the $B = 11$ G and $B = 0$ G cases is for the EEPFs measured at the axis. With the magnetic field, the EEPF departs from Maxwellian and has a large fraction of electrons with energies above the first ionization potential for argon (15.75 eV). This is in contrast to the case without the magnetic field, where the EEPF is closer to Maxwellian with the $T_e \approx 5$ eV and the energy cutoff below 30 eV. These differences between the two discharge cases can be attributed to the confinement of energetic electrons by the magnetic field in the radial direction (i.e. in the direction to the electron attractive chamber wall which is at the anode potential, Fig. 1). In the axial direction along the magnetic field lines, electrons are bouncing between the cathode and the electron-repelling plasma-wall sheath formed at the surface of the dielectric wall facing the plasma and intersected by the axial magnetic field [20]. The overall result of these plasma processes is a much larger plasma density obtained in the vicinity of the centerline of the plasma reactor with the magnetic field. For example, the plasma density measured at the chamber axis is 6 times larger with the magnetic field than without the magnetic field (e.g. $n_e \approx 6 \cdot 10^{11} \text{ cm}^{-3}$ vs. $n_e \approx 1 \cdot 10^{11} \text{ cm}^{-3}$). At the distance of 10 cm from the axis, the EEPFs with and without the magnetic field are similar. For both cases, the plasma density and the effective electron temperature at the plasma periphery region are $(7\text{--}8) \cdot 10^9 \text{ cm}^{-3}$ and 4.7–4.8 eV, respectively.

There are three important implications of the above results of plasma measurements. First, the energy of ions impinging on the graphene surface placed on the floating substrate is determined by the potential drop at the plasma-sample interface. For plasma with Maxwellian EEPF, the sheath potential drop at the planar floating wall can be expressed using well-known expression [31] $\Delta V \approx T_e \ln(0.61 \sqrt{2\pi m_e/M})$, where m_e and M are the electron mass and the mass of a bombarding ion (Ar, H). Argon ions are heavier than carbon atoms and therefore, can cause a stronger sputtering of the graphene than hydrogen. Then, using the above results for the local electron temperature the sheath voltage drop is $\Delta V \sim 25$ V. Thus, at graphene, the Ar ion energy acquired by an electrostatic acceleration in the sheath should not exceed 25 eV. This energy is lower than the energy threshold for an Ar ion to displace a carbon atom in

a suspended graphene sheet, 31.2 eV [35, 36]. Thus, under experimental conditions of this discharge, the Ar ions do not have enough energy to induce irreversible damage to the graphene. Secondly, the ion flux to the floating substrate is likely small because it is in the opposite direction to the applied electric field and the density of the cylindrical plasma column drops significantly at the plasma periphery, at the location of the samples. Thirdly, the above plasma measurements also imply that with the magnetic field, there are larger gradients in the plasma density and the electron temperature along the radial direction than without the magnetic field. However, these results cannot directly explain the differences in the graphene hydrogenation coverage results with and without the magnetic field. A plausible explanation of these differences in the graphene hydrogenation is that with the magnetic field, a larger fraction of energetic electrons generates more hydrogen atoms by the dissociation of hydrogen molecules than that without the magnetic field. This explanation, which is consistent with the EEPF measurements, is supported by the OES measurements [36]. In particular, for the case with the magnetic field, we measured more than 10 times larger intensity of hydrogen H-alpha ($H\alpha$), which is a specific deep-red visible spectral line in the Balmer series with a wavelength of 656.28 nm, compared to the $H\alpha$ intensity without the magnetic field, shown in Fig. S5. At the operating pressure of 11 mtorr, the mean free path of hydrogen atoms in the background Ar/H₂ gas, λ_{mfp} , is comparable with the distance between the electron beam region (the central region of the plasma reactor) and the graphene samples, L , $\lambda_{mfp} = 1/n\sigma \sim L$, where n is the density of the background gas and σ is the collisional cross-section area ($\sigma \sim \pi(R_{Ar} + R_H)^2$, where R_{Ar} , R_H are radii of Ar and H atoms, respectively). Thus, hydrogen atoms generated at the electron beam region of the plasma reactor should be able to reach the sample surface without collisions with the background gas.

Finally, the results of plasma-induced hydrogen coverage on graphene from different studies, including this work, are highlighted in Table 2. Higher hydrogen coverage results are obtained by plasma with an applied magnetic field. The low-temperature cross-field discharge plasma used in the present study provides a promising high hydrogen coverage on graphene with a long-duration and low-damage treatment.

4. Conclusions

In conclusion, the plasma discharge with applied crossed electric and magnetic fields generates the flux of hydrogen atoms enabling low damage hydrogenation on an atomically thin 2D material, graphene. Plasma measurements revealed that the application of the magnetic field allows to confine a larger fraction of energetic electrons in the plasma which generates more hydrogen atoms and ions than that without the magnetic field. The Raman spectra and the XPS spectra investigation demonstrates that this cross-field plasma provides a promising way to achieve higher hydrogen coverage than other reported plasma methods. Due to the lower hydrogen barriers of multi-layer graphene, the hydrogen coverages on the bi-layer and tri-layer graphene are higher than that on the monolayer graphene.

In addition, our plasma measurements explain low damage induced by the ions to the 2D thin films. The main reasons are in 1) a relatively low local electron temperature which determines the voltage drop between the plasma and the floating samples - the plasma ions accelerated by this voltage drop fail to acquire enough energy to displace the carbon atoms in the graphene; 2) a low plasma density at the periphery of the cylindrical plasma column that implies a flux of low energy ions, and 3) the direction of the applied electric field that accelerates plasma generated ions away

Table 2
Comparison of hydrogenated graphene by plasma from different groups.

Sample	Plasma	Gas Source	Duration	Dehydrogenation Annealing ^a	Hydrogen coverage	Reference
Exfoliated graphene	DC	Ar/H ₂ (9:1)	120 min	Yes	10%	15
Exfoliated graphene	RF	H ₂	1 min	Yes	16.67%	12
CVD graphene	Microwave	H ₂	20 min	Yes	25%	27
CVD graphene	RF with a magnetic field	H ₂	2 s	No	33%	16
CVD graphene	Electron beam with a magnetic field	Ar/H ₂ (19:1)	60 s	No	33%	17
CVD graphene	DC-RF with a magnetic field	Ar/H ₂ (4:1)	30 min	Yes	35.8%	this work

^a Confirm if the reference provides a dehydrogenation annealing process to demonstrate the graphene damage situation.

from the samples towards the reactor chamber axis. The low damage of graphene samples allowed a relatively long treatment time (30 min) that contributes to the high coverage obtained in these experiments. Thus, the low damage and high coverage plasma treatment make this low-temperature fine-tunable plasma-based source of hydrogen atoms attractive for use in functionalizing thin films, delivering modified 2D materials more exciting and up-and-coming for vast applications. One potential application of the cross-field plasma is to dope transition metal dichalcogenides as highly active catalysts for energy conversion.

CRediT authorship contribution statement

Fang Zhao: Term, Conceptualization, Resources, Methodology, Data curation, Formal analysis, Writing – original draft, Writing – Review & Editing. **Yevgeny Raiteses:** Conceptualization, Supervision, Formal analysis, Writing – original draft, Writing – review & editing, Funding acquisition. **Xiaofang Yang:** Methodology. **Andi Tan:** Writing – review & editing. **Christopher G. Tully:** Supervision, Project administration, Funding acquisition, Writing– Review & Editing. ‡ These authors contributed equally.

Declaration of competing interest

The authors declare that they have no known competing financial interests or personal relationships that could have appeared to influence the work reported in this paper.

Acknowledgments

F. Z., A.T. and C. T. acknowledge support from Simons Foundation (#377485), John Templeton Foundation (#58851). Y. R. acknowledges assistance of Sophia Gershman of PPPL with spectroscopic measurements. The work on plasma characterization of the source done by Y. R. was conducted at PPPL with support by the US DOE, Office of Science, Fusion Energy Sciences, under contract DE-AC02-09CH11466. The Penning source was built with support of the the Air Force Office of Scientific Research (FA9550-17-1-0010). The authors acknowledge the use of Princeton's Imaging and Analysis Center, which is partially supported by the Princeton Center for Complex Materials, a National Science Foundation (NSF)-MRSEC program (DMR-1420541).

Appendix A. Supplementary data

Supplementary data to this article can be found online at <https://doi.org/10.1016/j.carbon.2021.02.084>.

References

- [1] K.S. Novoselov, A.K. Geim, S.V. Morozov, D. Jiang, Y. Zhang, S.V. Dubonos, et al., Electric field effect in atomically thin carbon films, *Science* 306 (2004) 666–669.
- [2] J.S. Brunch, A.M. van der Zande, S.S. Verbridge, I.W. Frank, D.M. Tanenbaum, J.M. Parpia, et al., Electromechanical resonators from graphene sheets, *Science* 315 (2007) 490–493.
- [3] F. Xia, T. Mueller, Y.M. Lin, A. Valdes-Garcia, P. Avouris, Ultrafast graphene photodetector, *Nat. Nanotechnol.* 4 (2009) 839–843.
- [4] F. Schwierz, Graphene transistors, *Nat. Nanotechnol.* 5 (2010) 487–496.
- [5] K.S. Novoselov, A.K. Geim, S.V. Morozov, D. Jiang, M.I. Katsnelson, I.V. Grigorieva, et al., Two-dimensional gas of massless Dirac fermions in graphene, *Nature* 438 (2005) 197–200.
- [6] R.A. Nistor, D.M. News, G.J. Martyna, The role of chemistry in graphene doping for carbon-based electronics, *ACS Nano* 5 (2011) 3096–3103.
- [7] J. Zhou, Q. Wang, Q. Sun, X.S. Chen, Y. Kawazoe, P. Jena, Ferromagnetism in semihydrogenated graphene sheet, *Nano Lett.* 9 (2009) 3867–3870.
- [8] R. Balog, B. Jørgensen, J. Wells, E. Laegsgaard, P. Hofmann, F. Besenbacher, et al., Atomic hydrogen adsorbate structures on graphene, *J. Am. Chem. Soc.* 131 (2009) 8744–8745.
- [9] X. Li, X. Wang, L. Zhang, S. Lee, H. Dai, Chemically derived, ultrasmooth graphene nanoribbon semiconductors, *Science* 319 (2008) 1229–1232.
- [10] W. Yuan, J. Chen, G. Shi, Nanoporous graphene materials, *Biochem. Pharmacol.* 17 (2014) 77–85.
- [11] A. Castellanos-Gomez, M. Wojtaszek, Arramel, N. Tombros, B.J. Van Wees, Reversible hydrogenation and bandgap opening of graphene and graphite surfaces probed by scanning tunneling spectroscopy, *Small* 8 (2012) 1607–1613.
- [12] Z. Luo, T. Yu, K. Kim, Z. Ni, Y. You, S. Lim, Z. Shen, S. Wang, J. Lin, Thickness-dependent reversible hydrogenation of graphene layers, *ACS Nano* 3 (2009) 1781–1788.
- [13] D. Smith, R.T. Howie, I.F. Crowe, C.L. Simionescu, C. Murny, V. Vishnyakov, et al., Hydrogenation of graphene by reaction at high pressure and high temperature, *ACS Nano* 9 (2015) 8279–8283.
- [14] M.K. Rehm, Y.B. Kalyoncu, M. Kisiel, N. Pasher, F.J. Giessibl, F. Muller, et al., Characterization of hydrogen plasma defined graphene edges, *Carbon* 150 (2019) 417–424.
- [15] D.C. Elias, R.R. Nair, T.M.G. Mohiuddin, S.V. Morozov, P. Blake, M.P. Halsall, et al., Control of graphene's properties by reversible hydrogenation: evidence for graphene, *Science* 323 (2009) 610–613.
- [16] P. Gowda, D.R. Mohapatra, A. Misra, Enhanced photoresponse in monolayer hydrogenated graphene photodetector, *ACS Appl. Mater. Interfaces* 6 (2014) 16763–16768.
- [17] P.E. Hokins, M. Baraket, E.V. Barnat, T.E. Beechem, S.P. Kearney, J.C. Duda, et al., Manipulating thermal conductance at metal-graphene contacts via chemical functionalization, *Nano Lett.* 12 (2012) 590–595.
- [18] E. Rodriguez, V. Skoutnev, Y. Raiteses, A. Powis, I. Kaganovich, A. Smolyakov, Boundary-induced effect on the spoke-like activity in E x B plasma, *Phys. Plasmas* 26 (2019), 053503.
- [19] Y. Raiteses, I. Kaganovich, A. Smolyakov, Effects of the Gas Pressure on Low Frequency Oscillations in E X B Discharges, IEP-2015-307/ists-2015-B-307, Joint Conference of 30th International Symposium on Space Technology and Science 34th International Electric Propulsion Conference and 6th Nano-Satellite Symposium, Hyogo-Kobe, 2015, Japan July 4-10.
- [20] Y. Raiteses, J.K. Hendryx, N.J. Fisch, A parametric study of electron extraction from a low frequency inductively coupled RF-plasma source, IEP-2009-024, the 31st international electric propulsion conference, September 20 – 24, Ann Arbor, MI, 2009.
- [21] V. Skoutnev, P. Dourbal, E. Rodriguez, Y. Raiteses, Fast sweeping probe system for characterization of spokes in E x B discharge, *Rev. Sci. Instrum.* 89 (2018) 123501–123508.
- [22] S. Yatou, R.S. Selinsky, B.E. Koel, Y. Raiteses, “Synthesis-on” and “synthesis-off” modes of carbon arc operation during synthesis of carbon nanotubes, *Carbon* 125 (2017) 336–343.
- [23] J. Choi, S. Koo, M. Song, D.Y. Jung, S.Y. Choi, S. Ryu, Varying electronic coupling at graphene-copper interfaces probed with Raman spectroscopy, *2D Mater.* 7 (2020), 025006.
- [24] A.C. Ferrari, Raman spectroscopy of graphene and graphite: disorder, electron-phonon coupling, doping and nonadiabatic effects, *Solid State Commun.* 143 (2007) 47–57.
- [25] L. Chong, H. Guo, Y. Zhang, Y. Hu, Y. Zhang, Raman study of strain relaxation from grain boundaries in epitaxial graphene grown by chemical vapor deposition on SiC, *Nanomaterials* 9 (2019) 372.

- [26] D. Haberer, C.E. Giusca, Y. Wang, H. Sachdev, A.V. Fedorov, M. Farjam, et al., Evidence for a new two-dimensional C₄H-type polymer based on hydrogenated graphene, *Adv. Mater.* 23 (2011) 4497–4503.
- [27] J. Son, S. Lee, S.J. Kim, B.C. Park, H. Lee, S. Kim, et al., Hydrogenated monolayer graphene with reversible and tunable wide band gap and its field effect transistor, *Nat. Commun.* 7 (2016) 13261.
- [28] A. Kovtun, D. Jones, S. Dell'Elce, E. Treossi, A. Liscio, V. Palermo, Accurate chemical analysis of oxygenated graphene-based materials using X-ray photoelectron spectroscopy, *Carbon* 143 (2019) 268–275.
- [29] D. Ferrah, O. Renaut, D. Marinov, J. Arias-Zapata, N. Chevalier, D. Mariolle, et al., CF₄/H₂ plasma cleaning of graphene regenerates electronic properties of the pristine material, *ACS Appl. Nano Mater.* 2 (2019) 1356–1366.
- [30] S. Hu, M. Lozada-Hidalgo, F.C. Wang, A. Mishchenko, F. Schedin, R.R. Nair, et al., Proton transport through one-atom-thick crystals, *Nature* 516 (2014) 227–230.
- [31] P.Z. Sun, Q. Yang, W.J. Kuang, Y.V. Stebunov, W.Q. Xiong, J. Yu, et al., Limits on gas impermeability of graphene, *Nature* 579 (2020) 229–232.
- [32] D.Y. Zemlyanov, M. Jespersen, D.N. Zakharov, J. Hu, R. Paul, A. Kumar, et al., Versatile technique for assessing thickness of 2D layered materials by XPS, *Nanotechnology* 29 (2018) 115705.
- [33] M. Amjadipour, J. MacLeod, J. Lipton-Duffin, A. Tadich, J.J. Boeckl, F. Iacopi, N. Motta, Electron Effective attenuation length in epitaxial graphene on SiC, *Nanotechnology* 30 (2019), 025704.
- [34] M. Xu, D. Fujita, J. Gao, N. Hanagata, Auger electron spectroscopy: a rational method for determining thickness of graphene films, *ACS Nano* 4 (2010) 2937–2945.
- [35] J.D. Swift, M.J.R. Schwar, *Electrostatic Probes for Plasma Diagnostics*, Elsevier, 1969.
- [36] P. Ahlberg, O.L. Johansson, Z.-B. Zhang, U. Jansson, S.-L. Zhang, A. Lindblad, T. Nyberg, Defect formation in graphene during low energy ion bombardment, *Apl. Mater.* 4 (2016), 046104.